Dual-Mode Soft-Transition Control for Single-Phase Grid-Connected Photovoltaic Inverters

David Elizondo, Andoni Urtasun
Department of Electrical, Electronic and Communication Engineering
Institute of Smart Cities
Public University of Navarra (UPNA)
Pamplona, Spain

***Abstract*— Single-phase grid-connected inverters for photovoltaic power generation have been strongly analysed for improvement. Dual-mode control for two-stage inverters makes it possible to improve the efficiency by alternating between switching the dc/dc boost and the dc/ac buck stages, depending on the grid voltage value. However, according to the literature, the transition from one mode to the other is abrupt, which harms the grid current quality. This paper proposes a dual-mode control method which achieves high efficiency and a soft-transition in the grid current. Applying suitable feed-forward compensations, this control method improves the grid current quality, as demonstrated by the presented simulation results.**

Keywords—Dual-mode control, soft transition, grid current quality, feed-forward compensations, single-phase photovoltaic converter.

I. INTRODUCTION

Small-scale grid-connected PV systems are no longer interesting only from the environmental point of view [1], but also from the economical point of view: utility-scale systems reached grid parity by 2013 in several countries such as Australia, Germany, Netherlands and Italy [2]. These power generation systems often use single-phase grid-connected converters consisting of two power stages (DC-DC boost and DC-AC buck stages).

Traditionally, small-scale grid-connected converters have been controlled by a cascaded control loop for each power stage, with an external voltage loop and an internal current loop [3]–[5]. While boost stage cascaded loop controls input voltage (v_{in}) and boost current (i_{L1}), buck stage cascaded loop controls DC-link voltage (v_{dc}) and grid current (i_{L2}). Another characteristic of traditional control is that both power conversion stages (boost stage and buck stage) work at high frequency, which affects converter efficiency [6]. This fact goes against the main goal of small-scale grid-connected PV systems: to maximize the profit by reducing the installation costs and increasing the system efficiency. Taking this into account, for several years, researches on this matter have focused on developing high efficient, smaller and lighter PV converters [1], [6], [7].

One of the most analysed and discussed lines of research considers the converter efficiency improvement from the control point of view [1], [6]–[10]. Many of them are based on the dual-mode operation principle. The improvement in efficiency has been demonstrated [1], [6]–[8], [10]. However, the transition between one operating mode and the other appears to be rather rough due to the way the change is made in the control. This abrupt transition affects the grid current quality and implies low-frequency harmonics.

This work was supported by the Spanish State Research Agency (AEI) and FEDER-UE under grant DPI2016-80641-R.

In this paper, a control method for a dual-mode soft-transition inverter is proposed. The control method directly controls the grid current in both modes by applying the appropriate feed-forward compensations for each operating mode, thus achieving soft-transition and high-quality current. Furthermore, the proposed system accomplishes fast dynamic response. The presented simulation results validate the proposed control.

The conversion topology represented in Fig. 1 is the one considered in this paper. It consists of a DC-DC boost converter and a full-bridge single-phase inverter connected to the grid. In order to increase efficiency in Buck operation mode, an ultrafast reverse recovery diode is added in the boost stage [1]. The main features of the converter are shown in Table I.

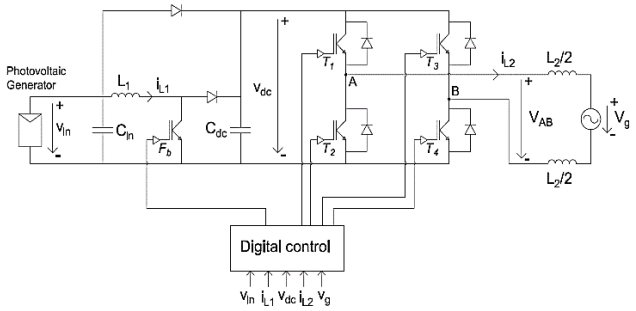

Fig.1. Conversion topology.

TABLE I. DESIGN PARAMETERS

Parameter	Value
Rated Power	6 kW
Input Voltage Range	150 V - 300 V
Grid frequency	50 Hz
Grid Voltage	230 V (rms)
Switching Frequency	16 kHz
Input Capacitor, C_{in}	9.8 mF
Boost Inductance, L_1	50 μH
DC Bus Capacitor, C_{dc}	10 μF
Inverter Output Inductance, L_2	2 mH

As can be observed in the table, the electrolytic capacitor that filters the harmonics at twice the grid frequency is placed at the input − in contrast with traditional control topology −, while C_{dc} and L_1 have very low values.

II. DUAL-MODE OPERATION PRINCIPLE

Dual-mode control strategy consists of the converter working in such a way that only one of its power stages – DC/DC boost or DC/AC buck – is switching. Therefore, two different operating modes can be defined: Buck mode and Boost mode. The transition from one mode to the other depends on the voltage grid instantaneous value, v_g.

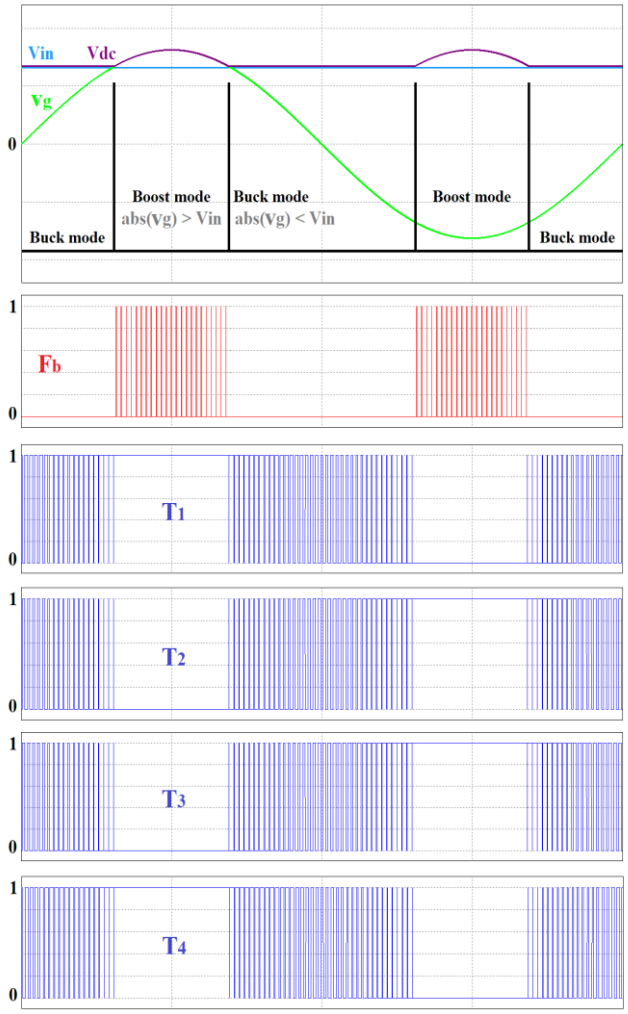

Fig. 2. Dual-mode operation principle and PWM signals.

Fig. 2 illustrates the dual-mode operation principle, representing both modes as well as the IGBT gate pulse sequences. As defined in Fig. 1, F_b is the boost PWM signal and T_1-T_4 are the buck PWM signals.

As can be observed in Fig. 2, when the DC input voltage, v_{in}, is higher than the absolute value of the voltage grid, the converter works in Buck mode. In this mode, only the inverter operates at high frequency with unipolar modulation – thus, its modulation signal, m, being a sinusoidal waveform –, while boost stage is not switching.

Then, when the DC input voltage is lower than the absolute value of the voltage grid, the converter performs in Boost mode and the boost stage is the one that operates at high frequency. In that case, the boost IGBT duty cycle, d, has a sinusoidal shape, while m is $+1$ (when $v_g > 0$) or -1 (when $v_g < 0$).

III. PROPOSED CONTROL

A. *Introduction to the proposed control*

The proposed control method (schematically depicted in Fig. 3) is based on dual-mode operation principle. As shown in the block diagram, there is an outer loop to control input voltage, v_{in}, and an inner loop which controls grid current, i_{L2}. As represented in Fig. 3, input voltage reference is determined by a MPPT algorithm. Then, voltage control loop defines the reference for current control loop. Finally, current control loop obtains both boost duty cycle, d, and buck modulation signal, m.

Taking into account that the implemented input voltage control loop is similar to the traditional [11], which is widely known, this paper focuses on the grid current control loop.

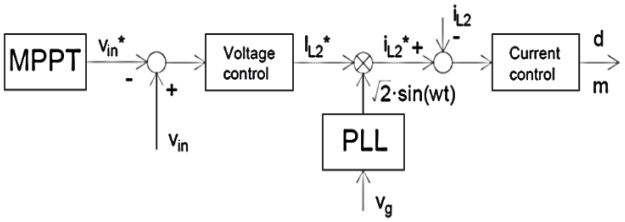

Fig. 3. Block diagram of the complete control system.

The proposed dual-mode current control is schematically shown in Fig. 4. As can be observed, the universal current controller, valid for both modes, obtains the necessary voltage at the output of the inverter (v_{AB}^*). Then, both control signals required to achieve $v_{AB} = v_{AB}^*$ are obtained, that is $m = v_{AB}^*/v_{dc}$ in Buck mode, and $1 - d = v_{in}/|v_{AB}|$ in Boost mode. Finally, $1 - d$ and $|m|$ are compared. The lowest value defines the operation mode and is imposed to the corresponding stage. The comparison between the inverter modulation signal and the boost duty cycle allows the current control to establish the corresponding mode (Boost or Buck) directly, being more accurate than comparing v_{in} and $|v_g|$. In case the operating mode is Boost mode ($|m| > 1 - d$), the boost duty cycle is a sinusoidal waveform, while $m = 1$ with positive grid voltage or $m = -1$ with negative grid voltage. If $|m| < 1 - d$, the converter operates in Buck mode, with the inverter stage working at high frequency with a sinusoidal modulation signal, while the Boost stage maintains $d = 0$.

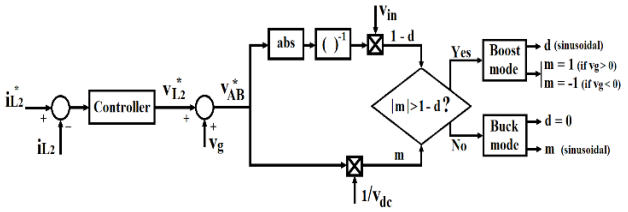

Fig. 4. Block diagram of the proposed dual-mode current control.

In order to analyse the current response under this control method and design the controller, small-signal models of Buck and Boost current plants are obtained. Then, the paper explains the proposed feed-forward compensations with the purpose of achieving soft transition and enough control loop speed and stability.

B. Buck mode

While working in Buck mode, the IGBT boost stage does not switch and the full-bridge inverter is switching at 16 kHz. As a result, the converter equivalent circuit is the one shown in Fig. 5. The bypass diode short-circuits the boost inductance.

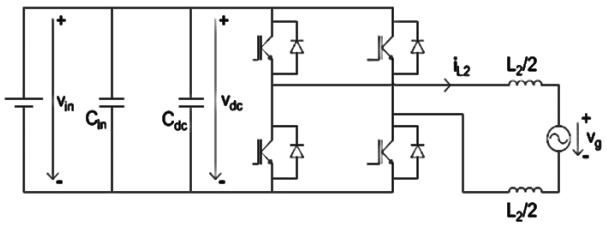

Fig. 5. Equivalent circuit in Buck mode.

The control-to-grid current plant is [5]

$$\frac{\hat{i}_{L2}(s)}{\hat{v}_{L2}(s)} = \frac{1}{L_2 \cdot s + R_2}, \tag{1}$$

where R_2 is the resistance of the inverter output inductance, L_2. As can be observed, it is a first-order system. Thus, Buck mode has a simple control-to-grid plant, so the controller would easily achieve convenient control loop dynamics and stability. However, since the same controller will be used for both modes, the Boost mode plant must be analysed before designing the controller.

C. Boost mode without feed-forward compensations

Fig. 6 represents the converter equivalent circuit when the converter is working in Boost mode. The split circuit shows how inverter stage sets the output voltage sign according to the grid voltage sign.

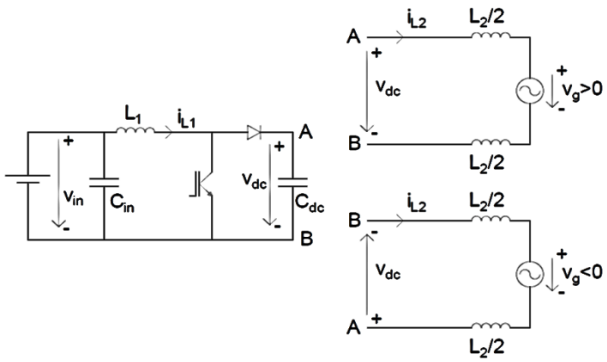

Fig. 6. Equivalent circuit in Boost mode.

The small-signal state-space representation for the converter can be obtained from the state equations [9], and results in (2), where R_1 and R_2 are the resistances of L_1 and L_2 inductors, respectively. Input voltage, $\hat{v}_{in}$, can be considered as a disturbance because of the great input capacity value, C_{in}.

$$\begin{pmatrix} L_1 & 0 & 0 \\ 0 & L_2 & 0 \\ 0 & 0 & C_{dc} \end{pmatrix} \cdot \frac{d}{dt} \begin{pmatrix} \hat{i}_{L1} \\ \hat{i}_{L2} \\ \hat{v}_{dc} \end{pmatrix} =$$

$$= \begin{pmatrix} -R_1 & 0 & -(1-D) \\ 0 & -R_2 & 1 \\ (1-D) & -1 & 0 \end{pmatrix} \cdot \begin{pmatrix} \hat{i}_{L1} \\ \hat{i}_{L2} \\ \hat{v}_{dc} \end{pmatrix} + \begin{pmatrix} V_{dc} & 1 & 0 \\ 0 & 0 & -1 \\ -I_{L1} & 0 & 0 \end{pmatrix} \cdot \begin{pmatrix} \hat{d} \\ \hat{v}_{in} \\ \hat{v}_g \end{pmatrix} \tag{2}$$

Applying the Laplace transformation to (2), it results in

$$\begin{pmatrix} L_1 \cdot s + R_1 & 0 & 1-D \\ 0 & L_2 \cdot s + R_2 & -1 \\ -(1-D) & 1 & C_{dc} \cdot s \end{pmatrix} \cdot \begin{pmatrix} \hat{i}_{L1}(s) \\ \hat{i}_{L2}(s) \\ \hat{v}_{dc}(s) \end{pmatrix} =$$

$$= \begin{pmatrix} V_{dc} & 1 & 0 \\ 0 & 0 & -1 \\ -I_{L1} & 0 & 0 \end{pmatrix} \cdot \begin{pmatrix} \hat{d}(s) \\ \hat{v}_{in}(s) \\ \hat{v}_g(s) \end{pmatrix}. \tag{3}$$

Then, operating, the duty cycle-to-grid current transfer function in Boost mode is obtained as (4).

The duty cycle-to-grid current plant in Boost mode is represented in Fig. 7. The system in Fig. 7 is considered for $v_{in} = 150\,V$ – the minimum input voltage allowed –, standing as the input voltage value of interest because, in this case, duty cycle achieves maximum variation, dependent on the voltage grid at each moment, V_g. For this reason, duty cycle-to-grid current plant is plotted in Fig. 7 for three different operating points, represented by the grid voltage at three different moments, $V_g = 150, 240$ and $325\,V$.

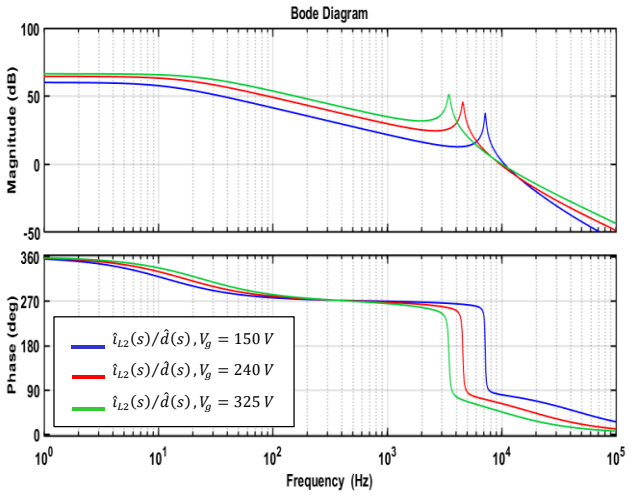

Fig. 7. Bode plot of duty cycle-to-grid current transfer function in Boost mode for $v_{in} = 150\,V$ and three different grid voltages.

$$\frac{\hat{i}_{L2}(s)}{\hat{d}(s)} = \frac{-L_1 I_{L1} s - R_1 I_{L1} + V_{dc}(1-D)}{L_1 C_{dc} L_2 s^3 + (L_2 R_1 + L_1 R_2) C_{dc} s^2 + \left(C_{dc} R_1 R_2 + L_2 (1-D)^2 + L_1\right) s + R_1 + R_2 (1-D)^2} \tag{4}$$

A resonance and a right-half plane zero can be observed in the third-order system of (4) and in Fig. 7. The zero takes place at high frequency and has little influence in the current control. However, resonance frequency and system gain are variable, clearly affecting the control feasibility.

In order to accomplish a satisfactory gain margin, the cross-over frequency must be well before the resonance at the critical point of operation ($V_g = 325\,V$, grid voltage at its peak value). However, in this case, the system would have low cross-over frequency for other operating points due to the variable magnitude. As a result, the direct control of the grid current in Boost mode seems unfeasible with both enough stability margin and cross-over frequency for all operating points [9]. For this reason, it is proposed to apply feed-forward compensations.

D. Boost mode with feed-forward compensations

The block diagram of the control with feed-forward compensations in Boost mode was shown in Fig. 4. Thus, the duty cycle in this mode is obtained as

$$d = 1 - \frac{v_{in}}{v_{L2} + v_g} \Rightarrow \frac{\hat{d}(s)}{\hat{v}_{L2}(s)} = \frac{1-D}{V_{L2} + V_g} = \frac{1-D}{V_{dc}}. \qquad (5)$$

Taking into account this compensation, the control-to-grid current transfer function becomes (6) and is represented in Fig. 8 for $v_{in} = 150\,V$ and for the same three operating points of Fig. 7.

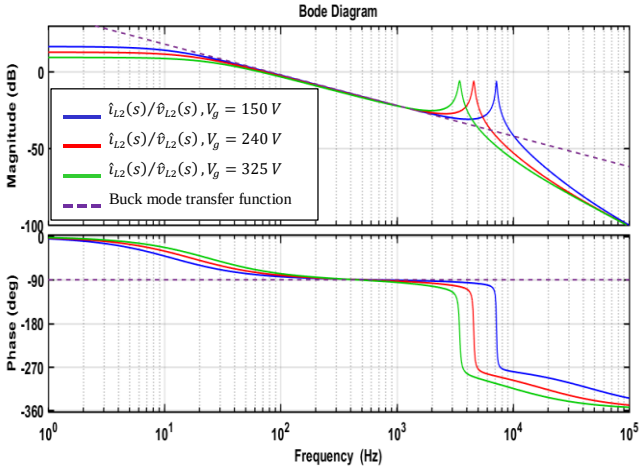

Fig. 8. Bode plot of control-to-grid current transfer function with feed-forward compensations in Boost mode for $v_{in} = 150\,V$ and three different grid voltages.

Thanks to the proposed feed-forward compensations, grid current direct control now becomes feasible. This fact allows to design a loop to directly control grid current in Boost mode – instead of controlling it indirectly, through the boost inductor current [9] – with enough speed and phase margin. Moreover, Fig. 8 shows that, in the frequency range of interest, the same magnitude and phase is obtained for the whole operating range. In this range – between 50 Hz and 2 kHz approximately – the control-to-grid current transfer function in Boost mode can be approximated as

$$\frac{\hat{i}_{L2}(s)}{\hat{v}_{L2}(s)} \approx \frac{1}{s \cdot L_2}, \qquad (7)$$

which is equivalent to the one in Buck mode (see (1)).

As a result, the same controller can be used for both operating modes, which helps to obtain a soft transition.

E. Grid current control loop

As demonstrated, Buck mode and Boost mode control-to-grid transfer functions are equivalent in a wide frequency range when the proposed feed-forward compensations are implemented in the control loop. This makes it possible to design a universal controller and, as represented in Fig. 4, to implement a single control loop for both Buck and Boost modes.

A type II controller (see (8)) is selected to reduce the peak resonance of the current plant. The current loop is designed to have a cross-over frequency of 500 Hz and a phase margin of 35º.

$$C_i = K_P \cdot \frac{T_n \cdot s + 1}{T_n \cdot s \cdot (s/\omega_p + 1)}, \qquad (8)$$

where C_i is the controller transfer function, K_P is the controller static gain, T_n is the controller time constant and ω_p is the pole frequency.

Once the controller has been designed, the open-loop transfer function is represented in Fig. 9. This transfer function includes the controller, the digital sampling delay, a current first-order filter with cutoff of 4 kHz, and the system plant. In the figure, four cases are represented: open-loop system in Boost mode for the same three operating points of Fig. 7 and Fig. 8, and open-loop system in Buck mode.

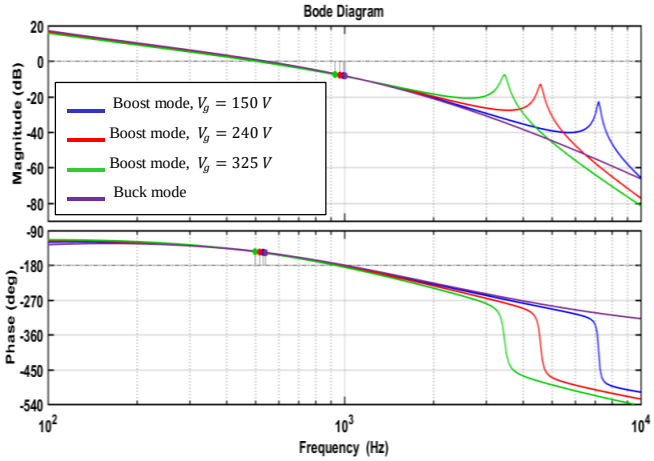

Fig. 9. Bode plot of open-loop system in Boost mode for $v_{in} = 150\,V$ and three different grid voltages, and in Buck mode.

As observed in the figure, the magnitude and phase in the range of interest is nearly the same for all operating points. As a result, cross-over frequency and phase margin are almost constant and vary between 500 and 542 Hz, and 35º and 32.5º,

$$\frac{\hat{i}_{L2}(s)}{\hat{v}_{L2}(s)} = \frac{-L_1 I_{L1}(1-D)s/V_{dc} - R_1 I_{L1}(1-D)/V_{dc} + (1-D)^2}{L_1 C_{dc} L_2 s^3 + (L_2 R_1 + L_1 R_2) C_{dc} s^2 + \left(C_{dc} R_1 R_2 + L_2 (1-D)^2 + L_1\right) s + R_1 + R_2 (1-D)^2} \qquad (6)$$

respectively. Fig. 9 also shows that gain margin always remains higher than 7.5 dB.

The closed-loop system is represented in Fig. 10. As in Fig. 9, the equivalence between Buck and Boost operating modes in the frequency range of interest can be observed.

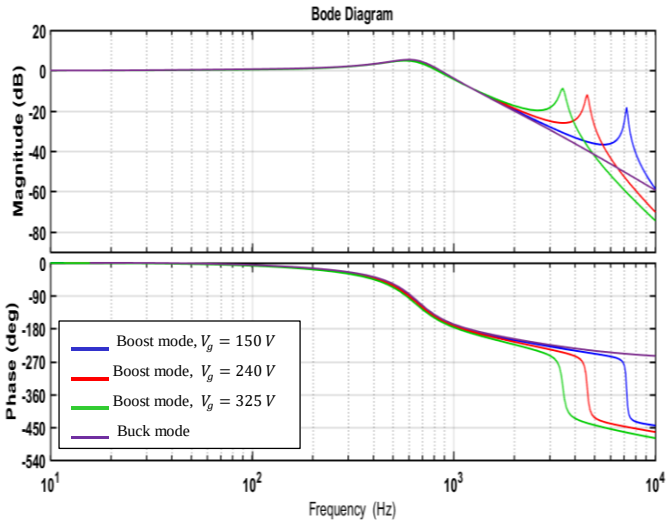

Fig. 10. Grid current closed-loop system in Boost mode for $v_{in} = 150\ V$ and three different grid voltages, and in Buck mode.

IV. SIMULATION RESULTS

The adequate behaviour of the proposed control method is proved on the basis of computer simulation using PSIM software. The simulation considers the converter shown in Fig. 1 and a digital control consisting of the control loops schematically represented in Fig. 3 and Fig. 4.

The grid current and control signals $1 - d$ and m are shown in Fig. 11, where Fig. 11 (a) represents them when the inverter operates at MPP, that is, $v_{in} = 263\ V$. The total harmonic distortion factor of the output current is 1.11%. This low THD value, together with the absence of abrupt transition in the current waveform, proves that high-quality grid current has been achieved.

Fig. 11 (b) represents grid current and control signals for the minimum input voltage, $v_{in} = 150\ V$. In this case, output current THD is 3.84%. As can be observed, also in this case a soft transition between modes of operation is achieved and, as a result, the grid current is purely sinusoidal but for the switching ripple.

In order to evaluate the system dynamic response, current control loop is tested with a step in the grid current reference. This test considers an instantaneous reduction of the grid current reference, from 26.09 A (rms), corresponding to converter nominal power, to 13.04 A (rms). Results are shown in Fig. 12. While in Fig. 12 (a), grid current, current reference and control signals are shown when the step is simulated during Boost mode, in Fig. 12 (b) the same waveforms are represented when the current reference step is simulated during converter Buck mode.

As can be observed in Fig. 12, the control loop is stable and fast enough to adapt current output after a step in the current reference.

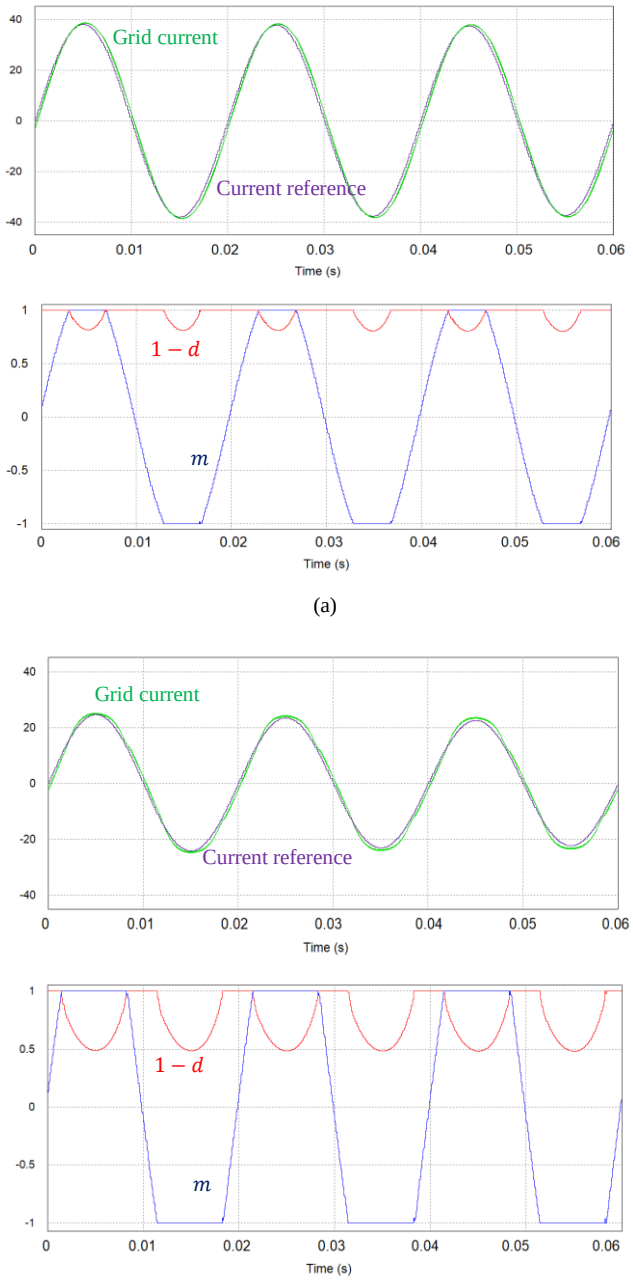

Fig. 11. Simulation results in steady-state operation: (a) $v_{in} = 263\ V$ (MPP); (b) $v_{in} = 150\ V$.

V. CONCLUSION

In this paper, a dual-mode soft-transition control method is proposed. High efficiency is ensured by the dual-mode operation of the converter. Thanks to the proposed control with only one controller for both modes and appropriate feed-forward compensations, a satisfactory current control is achieved. The simulation results show that the control technique succeeds in achieving a soft transition, thus injecting high quality current into the grid. Furthermore, the obtained results show that the designed control is very fast, with excellent dynamic response.

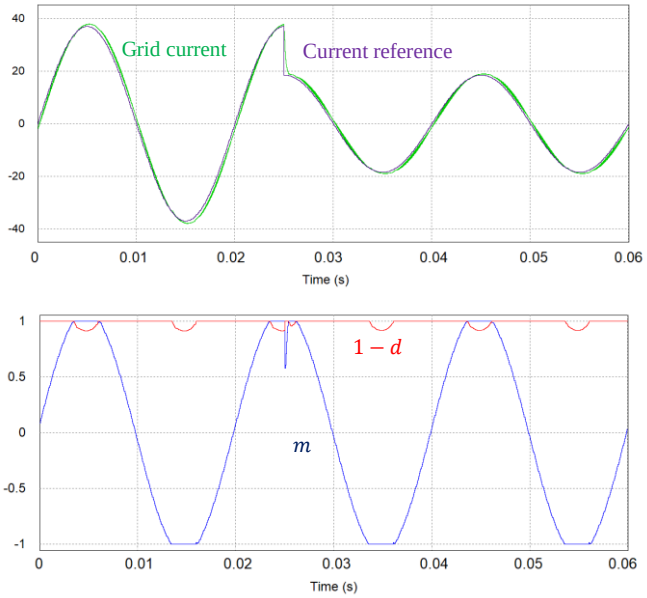

(a)

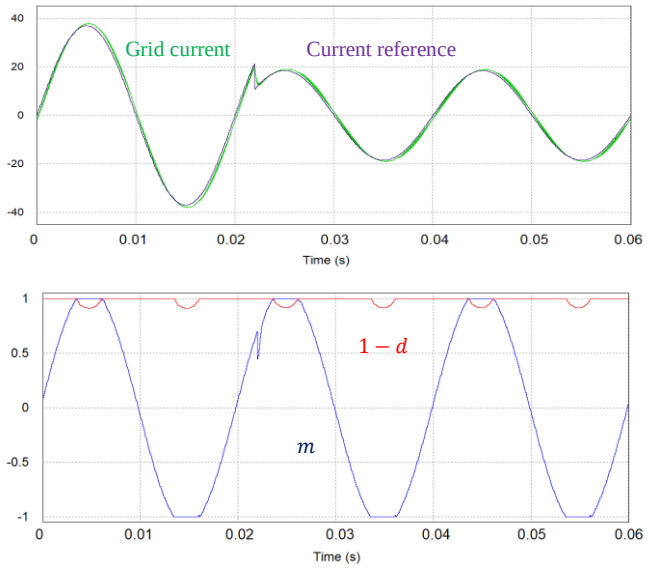

(b)

Fig. 12. Simulation results for reference step from nominal power output to 50% power output: (a) in Boost mode; (b) in Buck mode.

REFERENCES

[1] K. Ogura, T. Nishida, E. Hiraki, M. Nakaoka, and S. Nagai, "Time-sharing boost chopper cascaded dual mode single-phase sinewave inverter for solar photovoltaic power generation system," PESC Rec. - IEEE Annu. Power Electron. Spec. Conf., vol. 6, pp. 4763–4767, 2004.

[2] International Energy Agency IEA, *Technology Roadmap: Solar Photovoltaic Energy*, 2014.

[3] A. Urtasun, P. Sanchis, and L. Marroyo, "Adaptive voltage control of the DC/DC boost stage in PV converters with small input capacitor," IEEE Trans. Power Electron., vol. 28, no. 11, pp. 5038–5048, 2013.

[4] T. Hao, G. Feng, and C. Cong, "Advanced performance control of two-stage grid-tied photovoltaic inverter with fast energy storage component," Proc. - 2012 3rd IEEE Int. Symp. Power Electron. Distrib. Gener. Syst. PEDG 2012, pp. 403–409, 2012.

[5] H. C. H. Cha, T.-K. V. T.-K. Vu, and J.-E. K. J.-E. Kim, "Design and control of Proportional-Resonant controller based Photovoltaic power conditioning system," 2009 IEEE Energy Convers. Congr. Expo., pp. 2198–2205, 2009.

[6] W. Wu, J. Ji, and F. Blaabjerg, "Aalborg Inverter - A New Type of "Buck in Buck, Boost in Boost" Grid-Tied Inverter," IEEE Trans. Power Electron., vol. 30, no. 9, pp. 4784–4793, 2015.

[7] N. A. Ahmed, H. W. Lee, and M. Nakaoka, "Dual-mode time-sharing sinewave-modulation soft switching boost full-bridge one-stage power conditioner without electrolytic capacitor DC link," IEEE Trans. Ind. Appl., vol. 43, no. 3, pp. 805–813, 2007.

[8] Z. Zhao, M. Xu, Q. Chen, J. S. J. Lai, and Y. Cho, "Derivation, analysis, and implementation of a boost-buck converter-based high-efficiency PV inverter," IEEE Trans. Power Electron., vol. 27, no. 3, pp. 1304–1313, 2012.

[9] W. Wu, H. Geng, P. Geng, Y. Ye, and M. Chen, "A Novel Control Method for Dual Mode Time-Sharing Grid-Connected Inverter," Energy Convers. Congr. Expo., vol. 1, pp. 53–57, 2010.

[10] W. Wu and T. Tang, "Dual-mode time-sharing cascaded sinusoidal inverter," IEEE Trans. Energy Convers., vol. 22, no. 3, pp. 795–797, 2007.

[11] T. Messo, J. Jokipii, J. Puukko, and T. Suntio, "Determining the value of DC-link capacitance to ensure stable operation of a three-phase photovoltaic inverter," IEEE Trans. Power Electron., vol. 29, no. 2, pp. 665–673, 2014.